© 2019. Published by The Company of Biologists Ltd | Development (2019) 146, dev172858. doi:10.1242/dev.172858

TECHNIQUES AND RESOURCES

STEM CELLS AND REGENERATION ARTICLE

Dynamics of Wnt activity on the acquisition of ectoderm potency in epiblast stem cells

Pierre Osteil[1,2,¶], Josh B. Studdert[1], Hwee Ngee Goh[1], Emilie E. Wilkie[1,3], Xiaochen Fan[1], Poh-Lynn Khoo[1], Guangdun Peng[4,‡,§], Nazmus Salehin[1], Hilary Knowles[1], Jing-Dong J. Han[5], Naihe Jing[4], Nicolas Fossat[1,2,*] and Patrick P. L. Tam[1,2]

ABSTRACT

During embryogenesis, the stringent regulation of Wnt activity is crucial for the morphogenesis of the head and brain. The loss of function of the Wnt inhibitor Dkk1 results in elevated Wnt activity, loss of ectoderm lineage attributes from the anterior epiblast, and the posteriorisation of anterior germ layer tissue towards the mesendoderm. The modulation of Wnt signalling may therefore be crucial for the allocation of epiblast cells to ectoderm progenitors during gastrulation. To test this hypothesis, we examined the lineage characteristics of epiblast stem cells (EpiSCs) that were derived and maintained under different signalling conditions. We showed that suppression of Wnt activity enhanced the ectoderm propensity of the EpiSCs. Neuroectoderm differentiation of these EpiSCs was further empowered by the robust re-activation of Wnt activity. Therefore, during gastrulation, the tuning of the signalling activities that mediate mesendoderm differentiation is instrumental for the acquisition of ectoderm potency in the epiblast.

KEY WORDS: Epiblast stem cells, Lineage propensity, Wnt signalling, Neurogenesis, Head development

INTRODUCTION

The anterior-posterior patterning of the basic body plan of the vertebrate embryo is driven by the regionalised activity of a multitude of signalling pathways (Durston, 2015; Hikasa and Sokol, 2013; Petersen and Reddien, 2009; Robertson et al., 2003). During the morphogenesis of the embryonic head, the execution of the genetic program for the formation of major segments of the brain and the craniofacial primordia is underpinned by the stringent regulation of an anterior-posterior gradient of Wnt signalling activity (Fossat et al., 2011, 2012). This signalling gradient is generated by the combinatorial activity of the agonists, receptors, transducers and antagonists of the Wnt pathway (Eroshkin et al., 2016; Hikasa et al., 2010; Kiecker and Niehrs, 2001; Kim et al., 2002; Nakamura et al., 2008; Takata et al., 2017; Yukita et al., 2004). The notion of a Wnt activity gradient in the embryo is reinforced by the transcriptomic study of the late-gastrula stage embryo showing that the activity of the Wnt signalling pathway is enhanced in the posterior germ layers while being repressed in the anterior germ layers (Arkell and Tam, 2012). Correlative analysis of signalling activity and cell fates revealed that epiblast cells in the Wnt-active posterior domain are destined for the mesoderm and endoderm lineages, whereas those in the anterior Wnt-repressed domain are fated for the ectoderm (Engert et al., 2013; Peng et al., 2016; Takata et al., 2017). However, the exact role of Wnt signalling in cell fate decision remains to be elucidated.

Dkk1 encodes an extracellular inhibitor that antagonises the Wnt signalling activity. In the context of antagonistic activity, *Dkk1* targets the Kremen-LRP5/6 co-receptor complex (Mao et al., 2002). Once bound, it modulates the ligand-receptor interaction and signal transduction, establishing a regulatory loop that fine-tunes the level of Wnt signalling activity (Glinka et al., 1998; Krupnik et al., 1999). Gene expression analysis shows that *Dkk1* is expressed early in the anterior visceral endoderm (AVE) in the pre-/early-gastrula stage embryo (E6.5) and later in the nascent anterior axial mesendoderm in the vicinity of the anterior epiblast in the gastrula stage embryo (E7.0) (Fig. S1A,B) (Fossat et al., 2015; Glinka et al., 1998; Ip et al., 2014; Pearce et al., 1999; Peng et al., 2016; Pfister et al., 2007; Zakin et al., 2000). The temporal and tissue-specific pattern of *Dkk1* activity is consistent with its role in modulating signalling activity in the anterior epiblast during gastrulation. In *Xenopus* embryo, overexpression of *Dkk1* results in an enlarged head and, in conjunction with BMP inhibition, the duplication of head structures (Glinka et al., 1998; Kazanskaya et al., 2000). Conversely, blocking *Dkk1* activity by inhibitory antibodies generates head-deficiency defects (Glinka et al., 1998; Semënov et al., 2001). In the mouse, the impact of the loss of *Dkk1* function is manifested as a complete truncation of the head (Mukhopadhyay et al., 2001; Fossat et al., 2011). The loss-of-function phenotype may not be associated with the loss of progenitor tissues, as there was no preponderant loss of cells from the anterior epiblast of the $Dkk1^{-/-}$ embryo at late gastrulation prior to the formation of the embryonic head (Fossat et al., 2012). Instead, the inability to modulate the Wnt activity may have disrupted the acquisition of the requisite ectoderm germ layer potency during the allocation of the anterior epiblast to the progenitor tissues of the embryonic head at gastrulation.

Epiblast stem cells (EpiSCs), which are pluripotent cells derived from the epiblast of the pre- and early-streak stage embryo (Brons et al., 2007; Tesar et al., 2007), progress *in vitro* to a state that is

[1]Embryology Unit, Children's Medical Research Institute, Westmead, NSW 2145, Australia. [2]School of Medical Sciences, Faculty of Medicine and Health, University of Sydney, Sydney, NSW 2006, Australia. [3]Bioinformatics Group, Children's Medical Research Institute, Westmead, NSW 2145, Australia. [4]State Key Laboratory of Cell Biology, Institute of Biochemistry and Cell Biology, Shanghai Institutes for Biological Sciences, Chinese Academy of Sciences, Shanghai 200031, China. [5]Key Laboratory of Computational Biology, CAS Center for Excellence in Molecular Cell Science, Collaborative Innovation Center for Genetics and Developmental Biology, Chinese Academy of Sciences-Max Planck Partner Institute for Computational Biology, Shanghai Institutes for Biological Sciences, Chinese Academy of Sciences, Shanghai 200031, China.
*Present address: Copenhagen Hepatitis C Program (CO-HEP), Department of Immunology and Microbiology, University of Copenhagen, and Department of Infectious Diseases, Hvidovre Hospital, Denmark. ‡Present address: CAS Key Laboratory of Regenerative Biology, Guangzhou Institutes of Biomedicine and Health, Chinese Academy of Sciences, University of Chinese Academy of Sciences, Guangzhou 510530, China. §Present address: Guangzhou Regenerative Medicine and Health GuangDong Laboratory (GRMH-GDL), Guangzhou 510005, China.

¶Author for correspondence (posteil@cmri.org.au)

P.O., 0000-0002-5832-6703; J.-D.J.H., 0000-0002-9270-7139

Received 17 October 2018; Accepted 11 March 2019

Development (2019) 146, dev172858. doi:10.1242/dev.172858

developmentally similar to the late-gastrulation epiblast (Kojima et al., 2014). EpiSCs are therefore amenable for modelling the transition of the epiblast from the pluripotent state to germ layer specification. In the present study, a gain of antagonistic function approach was taken by blocking signalling activity in EpiSCs to elucidate the impact of reducing Wnt activity on lineage allocation prior to the differentiation to embryonic germ layer derivatives. Chemical inhibitors, either inhibiting the production of Wnt factors or affecting the stability and activity of rate-limiting components (e.g. axin 2 and tankyrase1/2) of the β-catenin destruction complex, have been previously used to block Wnt signalling activity in EpiSCs (Kurek et al., 2015; Liu et al., 2017, 2018; Sugimoto et al., 2015; Sumi et al., 2013; Wu et al., 2015). Treatment with inhibitors, such as IWP2, IWR1 and XAV939, enhances the efficiency of derivation of EpiSCs and drives them to attain a stable state with homogenous expression of pluripotency factors such as Oct4 and Nanog. EpiSCs derived in the presence of IWR1 can be engrafted to the posterior epiblast more efficiently, suggesting that stem cells subjected to inhibition of Wnt activity are developmentally more compatible with the primitive-streak germ layers (Wu et al., 2015). However, in EpiSCs treated with IWR1 and XAV939, the expression of *Foxd3* and *Sox2* was elevated, which is consistent with enhanced pluripotency but also with an ectoderm fate (Liu et al., 2017; Sugimoto et al., 2015; Sumi et al., 2013). Furthermore, no enhancement in the expression of neuroectoderm genes was observed in EpiSCs derived by culturing embryonic stem cells (ESCs) in activin/FGF supplemented medium and treated with IWP2 for 48 h (Kurek et al., 2015) or in EpiSCs derived, from epiblast, initially in activin/FGF conditions but re-established as stable lines in the presence of IWP2 (Liu et al., 2018). It is unclear whether the difference in lineage outcome stems from the variation of the *in vitro* conditions or in the cellular origin of the EpiSCs. It is therefore imperative to conduct experiments on EpiSCs that are derived and maintained under standardised conditions to test the impact of signalling activity on the wiring of germ layer allocation.

In this study, we found that suppressing Wnt activity during the derivation of EpiSCs allows for the acquisition of ectoderm propensity by the EpiSCs prior to differentiation. We revealed that this lineage predisposition is maintained subsequently during differentiation. Then, we demonstrated that withholding Wnt activity from EpiSCs at the pluripotency state empowers the subsequent activation of Wnt signalling during the differentiation of ectoderm progenitors. In the context of the formation of the embryonic head, EpiSC specification experiments illustrate that the dysregulation of Wnt activity leads to aberrant allocation of ectoderm progenitors in the anterior epiblast. This may underpin the head truncation phenotype of *Dkk1*-null embryo. Our study showed that modulation of Wnt signalling activity is a key mechanistic requirement for specification of the ectoderm lineage and embryonic patterning during gastrulation.

RESULTS

Loss of the Wnt antagonist *Dkk1* results in the loss of ectoderm characteristics in the anterior germ layer tissue

Analysis of the spatial transcriptome of gastrulation-stage mouse embryos [Fig. S1A (Cui et al., 2018; Peng et al., 2016)] showed that *Dkk1* is expressed in the AVE (E6.5) and the anterior definitive endoderm (E7.0-E7.5), the posterior epiblast (E7.0) and the primitive streak (PS) (E7.5), but not in the anterior epiblast (Fig. S1B). The expression was the highest in the anterior visceral endoderm (AVE) and at an intermediate level in the posterior epiblast and the PS. We hypothesised that although the *Dkk1* activity may serve to tune the level of Wnt signalling activity globally in the posterior epiblast, the strong expression of *Dkk1* in the AVE is necessary to suppress Wnt activity more robustly in the anterior epiblast for lineage specification.

To test this hypothesis, we profiled the gene expression pattern by microarray analysis of the anterior and posterior halves of E7.75 $Dkk1^{-/-}$ mutant embryo (Mukhopadhyay et al., 2001) to identify genes that were differentially expressed in the mutant relative to the wild-type (WT) counterparts (Fig. 1A). The analysis revealed 30 downregulated and 34 upregulated genes in the $Dkk1^{-/-}$ anterior fragments when compared with wild-type anterior tissues, whereas the posterior fragments showed no significant changes in the gene expression profile (Fig. 1B, Table S1). In the mutant anterior tissues, the downregulated genes included those associated with Wnt pathway activity (*Shisa2*, *Fzd5*, *Wnt7b*, *Tie1* and *Cer1*), and others that were normally expressed in the wild-type anterior tissues (e.g. *Otx2*, *Pou3f1*, *Sox2*, *Foxd4*, *Slc7a3* and *Fgf5*) (Fig. S2). Among the upregulated genes were Wnt-related genes (*Sp5* and *Wnt2*) and genes usually expressed in the posterior epiblast (*Cdx2*, *Hoxa1*, *Hoxb1*, *Hoxb2*, *Tbx6*, *Twist1*, *Mesp1*, *Meis1* and *Meis2)* (Fig. S2 and Table S1 for full gene lists). These findings showed that the activity of anterior-related genes was reduced while that of posterior-related genes was enhanced in the anterior tissues of the $Dkk1^{-/-}$ embryo. The downregulated genes were associated with neurogenesis, whereas the upregulated genes were involved in embryonic patterning and the development of posterior mesoderm tissues (Fig. 1C). Therefore, loss of Dkk1 function led to the posteriorisation of the anterior germ layers.

The impact of the loss of Dkk1 function on the germ layer specification of the epiblast was further assessed in wild-type EpiSCs derived in activin A and FGF2-supplemented medium (EpiSC-AF) and in EpiSCs derived from $Dkk1^{-/-}$ E6.5 embryos (EpiSC-$AF^{Dkk1-/-}$) (Fig. 1D, Fig. S1C) (Maretto et al., 2003). A comparison of the transcriptome of EpiSC-$AF^{Dkk1-/-}$ with EpiSC-AF by RNA-seq analysis revealed 4426 differentially expressed genes (DEGs) (Fig. S1D). Analysis for enrichment of developmentally related ontologies revealed that downregulated genes in EpiSC-$AF^{Dkk1-/-}$ were enriched for neurogenesis and upregulated genes for epidermis, endoderm and mesoderm development (Fig. S1E). Examples of downregulated genes included those normally expressed in the anterior epiblast (*Dkk1*, *Otx2*, *Hesx1*, *Shh* and *Cer1*), in the PS [*Mixl1*, *Lhx1*, *T*, *Tdgf1* (*Cripto*) and *Gsc*], ectoderm-related genes (*Dcx*, *Fabp7*, *Neurod4*, *Foxd3* and *Gad2*) and Wnt-related genes (*Shisa2*, *Sp5* and *Lef1*). Conversely, the upregulated genes encompassed the posterior-related genes (*Gata3/4/6*, *Mybph*, *Ren1*, *Duoxa2*, *Hand1*, *Hoxd9*, *Igf2*, *Cdx2*, *Tead4*, *Cited1* and *Snai1*) (see Table S2 for the full list of genes).

To test whether the pattern of differential gene expression is correlated to the trajectory of lineage differentiation, we tracked the expression of lineage marker genes, including seven pluripotency-, 29 ectoderm-, 26 mesoderm- and 21 endoderm-related genes ('Cell Lineage Reporter Card' Fig. S1F and Table S3 for more details) during *in vitro* differentiation of the EpiSCs (Fig. 1E). Interestingly, EpiSC-$AF^{Dkk1-/-}$ cells followed a different trajectory of embryoid body (EB) differentiation from that of EpiSC-AF cells (Fig. 1F). We found that whereas the mutant EpiSCs were able to differentiate into the derivatives of three germ layers, they displayed an enhanced expression of mesoderm and endoderm markers (46% and 33% of the reporter genes, respectively) and a reduced expression of ectoderm markers prior to differentiation (31% of ectoderm reporter genes were downregulated) when compared with EpiSC-AF cells (Fig. 1G). Concomitantly, analysis of DEGs after 4 days of differentiation showed that EpiSC-$AF^{Dkk1-/-}$ did not trigger the

Development (2019) 146, dev172858. doi:10.1242/dev.172858

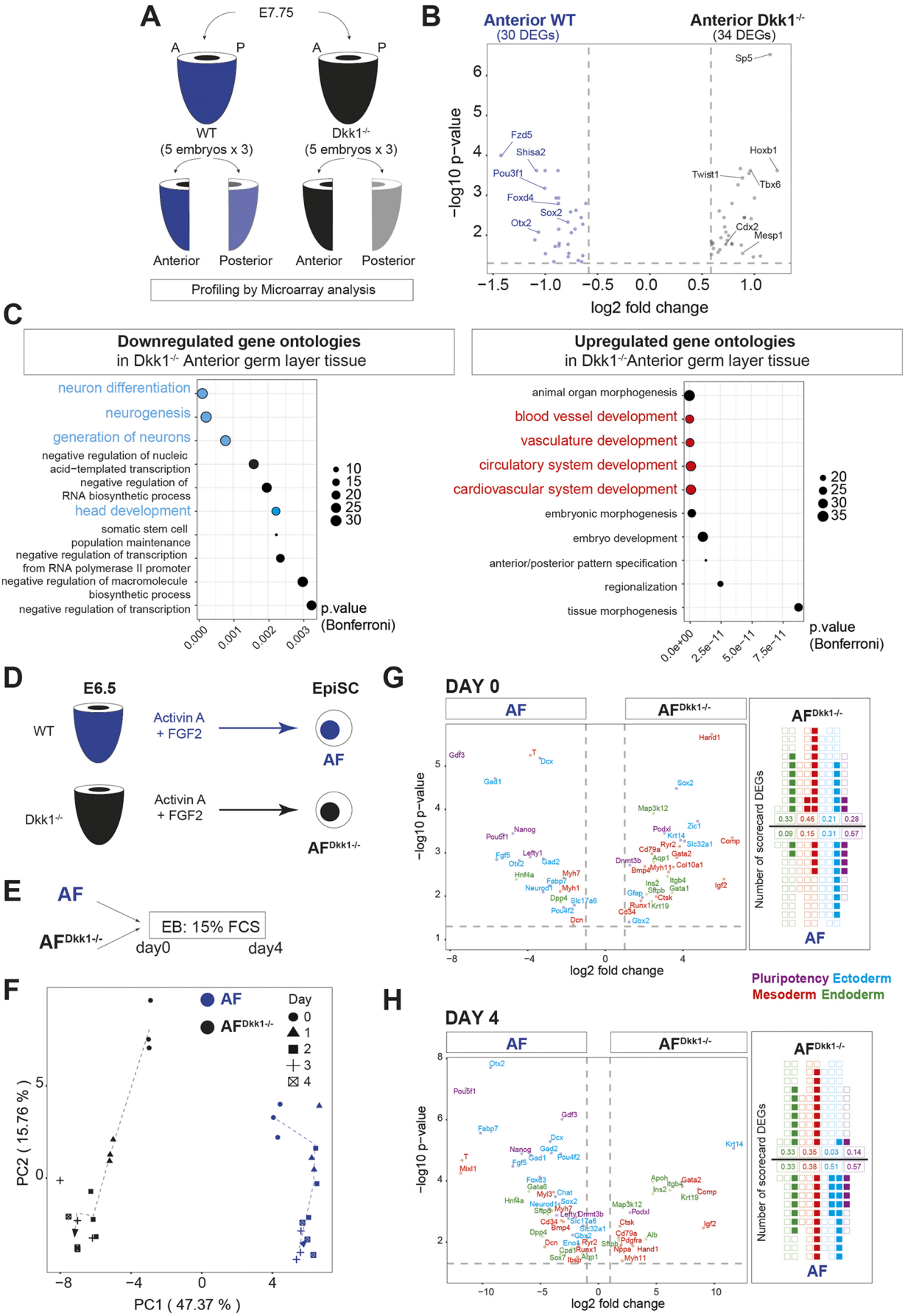

Fig. 1. See next page for legend.

Development (2019) 146, dev172858. doi:10.1242/dev.172858

Fig. 1. Transcriptomic profiling of *Dkk1*$^{-/-}$ E7.75 embryos and EpiSCs. (A) The workflow of microarray analysis of the anterior and posterior halves of wild-type (WT) and *Dkk1*$^{-/-}$ E7.75 early-bud stage embryos, collected in triplicate pools of five fragments each. (B) Volcano plot of the differentially expressed genes (DEGs) in the anterior germ layer tissue of the *Dkk1*$^{-/-}$ embryo relative to the anterior half of the wild-type embryo. Dashed lines represent the thresholds: fold change>1.5; P<0.05. (C) Top ontologies of downregulated and upregulated genes in *Dkk1*$^{-/-}$ anterior germ layer tissue. Dot size indicates the number of genes in each ontology with significance values (*x*-axis); blue, ontologies related to neurogenesis and head development; red, ontologies related to mesoderm differentiation. (D) Derivation of wild-type (AF) and *Dkk1*$^{-/-}$ (AF$^{Dkk1-/-}$) EpiSCs from the epiblast of E6.5 embryos in activin A- and FGF2-supplemented medium. (E) Illustration of the *in vitro* differentiation assay of EBs derived from EpiSC-AF and EpiSC- AF$^{Dkk1-/-}$ lines. The EBs were cultured in 15% FCS-supplemented medium for 4 days. Samples were collected every day for microfluidic qPCR analysis of gene expression. (F) PCA display of the trajectory of differentiation from day 0 to day 4 of *in vitro* culture of EBs derived from the EpiSC-AF and EpiSC- AF$^{Dkk1-/-}$ lines. EB differentiation was assessed by the expression of lineage reporter card genes (Fig. S1F) and the trajectory was constructed by connecting the centroid of replicates at successive time points (dotted arrows). Samples for each cell line were analysed in triplicate. Percentage in brackets indicates the variance proportion displayed in the first two PC axes. (G,H) Volcano plots of microfluidic qPCR data of differentially expressed lineage markers in AF and AF$^{Dkk1-/-}$ EBs at day 0 (G) and day 4 (H) of *in vitro* culture (samples in triplicate). *x*-axis, log2 fold change between EpiSC types; *y*-axis, -log10(*P*-value); dashed lines, thresholds at fold change>2 and P<0.05. Scorecard summary of the volcano plot data of differentially expressed lineage markers (scorecard DEGs) with each square representing a lineage marker; filled squares indicate DEGs in the specific EpiSC type: red, mesoderm; blue, ectoderm; green, endoderm; purple, pluripotency. The numbers underneath each group of genes represent the proportion of genes differentially expressed for each germ layer.

expression of ectoderm genes, except for *Krt14*: a surface ectoderm gene. This correlates perfectly with the RNA-seq analysis showing upregulation of genes of the mesendoderm and the surface ectoderm but not of neurogenesis (Fig. S1E). These results suggest that *Dkk1* activation is instrumental for neurogenesis.

To highlight the implication of loss of Dkk1 function on cell fate changes, we mapped the mutant germ layer tissues and the EpiSCs to the epiblast of a E7.5 embryo by correlation of the transcriptome (Zipcode analysis – see Materials and Methods for details) (Peng et al., 2016). *Dkk1*$^{-/-}$ anterior embryonic tissues did not match with the wild-type anterior epiblast but correlates more closely with the posterior-lateral epiblast (Fig. S1G, left panels). This finding suggested that *Dkk1*$^{-/-}$ anterior tissues had lost the characteristics of the anterior epiblast. In contrast, loss of Dkk1 function was immaterial to the lineage characteristics of the *Dkk1*$^{-/-}$ posterior epiblast (Fig. S1G, right panels). Consistent with the posteriorisation of the *Dkk1*$^{-/-}$ anterior tissues, EpiSC-AF$^{Dkk1-/-}$ cells matched more closely with the posterior epiblast, in contrast to the EpiSC-AF which matched with cell populations in the anterior and anterior-lateral epiblast (Fig. S1H). Therefore, ectopically elevated Wnt activity caused by the loss of *Dkk1* (Lewis et al., 2008) could lead to the loss of ectoderm potency of the anterior epiblast and impact negatively on the propensity to differentiate into ectoderm. The diminished ectoderm potency, particularly for neurogenesis, may underpin the defective development of fore- and mid-brain structures of the *Dkk1*$^{-/-}$ embryo (Fossat et al., 2011; Lewis et al., 2008; Mukhopadhyay et al., 2001).

Modulating Wnt activity in EpiSCs

To model the impact of Wnt activity on the germ layer potency of the epiblast, EpiSCs were derived from the epiblast of early-primitive-streak stage embryos in the presence of the Wnt inhibitor IWP2 (inhibitor of Wnt processing 2), activin A and FGF2 (Fig. 2A). IWP2 blocks Wnt signalling by inhibiting the activity of porcupine (an endoplasmic reticulum O-acyltransferase), which is necessary for processing Wnt proteins for secretion and the phosphorylation of the LRP6 receptor and DVL2 (Blauwkamp et al., 2012; Chen et al., 2009a). Therefore, the presence of IWP2 depletes the source of Wnt factors in the culture. After establishment, the EpiSCs were maintained in activin A/FGF2 medium supplemented with IWP2 (EpiSC-AFI cells). EpiSC lines derived from epiblast (Kojima et al., 2014) in medium containing activin A and FGF2 (EpiSC-AF cells, Fig. 1D) were used to model the effect of endogenous Wnt activity on epiblast specification and differentiation (Fig. 2A). To mimic the loss of Wnt antagonistic activity during epiblast differentiation in the *Dkk1*$^{-/-}$ embryo, sub-lines of EpiSC-AFI were switched to activin A/FGF2 medium without the inhibitor for more than six passages (EpiSC-AFI/AF) and, in parallel, cultured with recombinant Wnt3A for 24 h only (EpiSC-AFI+24W) (Fig. 2A, see Materials and Methods). Wnt activity was assessed in EpiSCs by the expression of a Tcf/Lef-lacZ reporter for the signalling response (Maretto et al., 2003). Fewer lacZ-positive cells were found in the EpiSC-AFI compared with EpiSC-AFI/AF cells (Fig. 2B). EpiSC-AFI cells also contained less total β-catenin and fewer cells displayed nuclear-localised active phosphorylated β-catenin than EpiSC-AFI/AF cells, suggesting that Wnt activity is reduced in the EpiSC-AFI cells (Fig. 2B). Western blot analysis showed that EpiSC-AFI cells have less active-β-catenin (ABC) compared with EpiSC-AF cells (Fig. 2C). To show that the signalling machinery was still functional, we treated the EpiSC-AFI cells with Wnt3A for 24 h. This short treatment led to accumulation of total-β-catenin, enhanced *Tcf-LacZ* expression (Fig. 2B), and increased level of ABC (Fig. 2C). EpiSCs were therefore responsive to exogenous Wnt signals and the IWP2 inhibitor did not change the functional competency of the signalling cascade aside from blocking the signalling activity elicited by endogenous ligands.

The pluripotency-related factors *Pou5f1* (*Oct4*) and *Nanog* were expressed in AF, AFI and AFI/AF EpiSCs (Fig. S3A). Quantification of the nuclear content of Pou5f1 and Nanog in individual cells revealed there were more AFI cells containing higher levels of Pou5f1 and Nanog proteins than AF and AFI/AF cells (Fig. S3B). Expression of pluripotency factors is therefore enhanced when Wnt activity is blocked, which is consistent with the findings of other EpiSC studies (Sugimoto et al., 2015; Sumi et al., 2013; Wu et al., 2015).

Inhibition of Wnt activity drives the predisposition for ectoderm differentiation

To characterise the molecular phenotype of EpiSCs derived and maintained under different conditions of Wnt activity, the transcriptomes of EpiSC-AF, EpiSC-AFI and EpiSC-AFI/AF cells were analysed by RNA-sequencing (Table S4). Relative to EpiSC-AF cells, more DEGs were unveiled in EpiSC-AFI cells (456 DEGs) (Fig. 2D, top panel) than in EpiSC-AFI/AF cells (247 DEGs) (Fig. 2E, top panel). Correlation analysis of DEG expression showed EpiSC-AFI/AF cells clustering with EpiSC-AF cells (Fig. S3C). We extracted 212, out of a total of 713 genes, that were uniquely differentially expressed across the three types of EpiSCs, of which 142 transcripts were validated for differential expression by microfluidic qPCR (Fig. S3D). These transcripts were encoded by genes related to lineage differentiation and Wnt signalling (see Table S5 for full gene list and data). Notably, the withdrawal of the inhibitor (EpiSC-AFI/AF) or supplementation of Wnt3A (EpiSC-

Development (2019) 146, dev172858. doi:10.1242/dev.172858

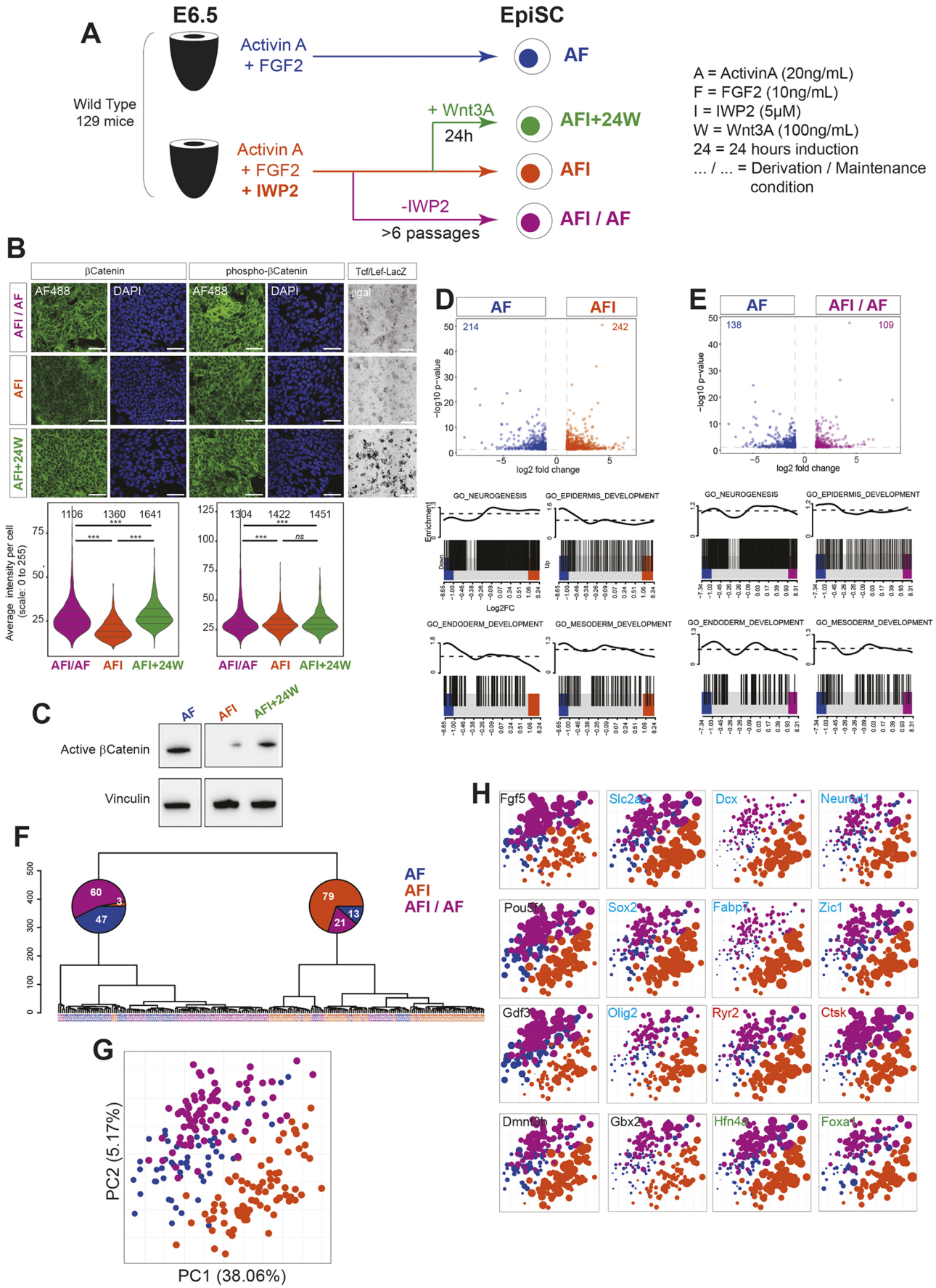

Fig. 2. See next page for legend.

Development (2019) 146, dev172858. doi:10.1242/dev.172858

Fig. 2. Generation and characterisation of EpiSC under different Wnt conditions. (A) Workflow of derivation and maintenance of the epiblast stem cells (EpiSCs) under different *in vitro* conditions: activin A and FGF2 (AF), the constant presence of IWP2 (AFI), established AFI cells maintained without IWP2 (AFI/AF) or with Wnt3A supplementation for 24 h (AFI+24W). (B) Intracellular content of total β-catenin and active phosphorylated β-catenin (phospho-βcatenin) assayed by immunostaining (nuclei are counterstained with DAPI). Scale bars: 50 µm. The response to Wnt signalling (Tcf/Lef-lacZ column) detected by the expression of the Tcf/Lef-lacZ reporter (X-gal staining). Scale bar: 100 µm. The quantification of nuclear content of total β-catenin (bottom left panel) and active phospho-β-catenin (bottom right panel) in AFI/AF, AFI and AFI+24W EpiSCs. Violin plots show the distribution of cell number (*x*-axis, cell line) and the intensity of immunostaining signal in the nucleus (*y*-axis). *P*-values were estimated using a Mann-Whitney-Wilcox non-parametric test: ***$P<0.001$; ns, non-significant. Numbers indicate the nuclei count for each condition. (C) Western blot for active-β-catenin in EpiSCs: AF, AFI and AFI+24W. Vinculin was used as a protein loading control. (D,E) RNA-seq analysis: volcano plots of the DEGs and barcode plots of the distribution of development-related genes in specific ontologies in (D) EpiSC-AFI and (E) EpiSC-AFI/AF relative to EpiSC-AF. The *x*-axis indicates the log2 fold change between EpiSC types; the y-axis indicates the -log10(*P*-value); dashed lines, thresholds at fold change>2 and $P<0.05$. Number of DEGs in each type of EpiSC is indicated in the top right or left corner. Lower panels: barcode plots indicate enrichment of genes of a particular ontology (neurogenesis, epidermis development, mesoderm development and endoderm development) in the different EpiSCs. Genes in the coloured area (blue, AF; purple, AFI/AF; orange, AFI) were significantly differentially expressed at FDR<0.05. Samples were analysed in duplicate. (F) Single-cell microfluidic qPCR. Hierarchical clustering analysis of single-cell qPCR data of AF, AFI and AFI/AF EpiSCs by the level of expression of 96 genes of the cell lineage reporter card (Fig. S1F). Pie charts showing the number of cells of each EpiSC line in the two main clusters. (G) PCA display of the clustering pattern of single cells of EpiSC-AF (blue), EpiSC-AFI/AF (purple) and EpiSC-AFI (orange) lines. Percentages in brackets indicate the variance proportion displayed by the first two PC axes. (H) Mapping of the gene expression level in individual single cells of EpiSC-AF, EpiSC-AFI and EpiSC-AFI/AF lines. PCA plots show the relative level of expression (represented by dot sizes) of genes related to ectoderm (blue), mesoderm (orange), endoderm (green) and pluripotency (black) in the single cells.

AFI+24W) reversed the expression of the majority of these DEGs (Fig. S3D,E). Removal of inhibition or provision of extrinsic Wnt signalling for the IWP2-treated EpiSCs had therefore reverted the transcriptomic signature to that of AF cells (Fig. S3E).

We interrogated the transcriptome for enrichment of genes in four developmentally related ontologies (neurogenesis, epidermis, endoderm and mesoderm development) in EpiSC-AFI/AF cells and EpiSC-AFI cells compared with EpiSC-AF cells. EpiSC-AFI cells were enriched for genes related to neurogenesis, and endoderm and mesoderm genes were under-represented (Fig. 2D, lower panel). The epidermis-related genes were not enriched in EpiSC-AFI cells, suggesting a selective role of Wnt inhibition in the specification of particular ectoderm derivatives. In contrast, EpiSC-AFI/AF cells did not display any enrichment (values ≈1) of any of the four ontologies relative to EpiSC-AF cells (Fig. 2E, lower panel).

To examine whether EpiSC-AFI cells has acquired a homogenous lineage property, single-cell RT-qPCR and clustering analysis were performed on 223 cells from the EpiSCs to profile the expression pattern of lineage-related genes (Table S5). EpiSCs segregated into two clusters: one enriched with EpiSC-AFI cells (79/113=70% cells in the cluster, representing 96% of EpiSC-AFI cells analysed) and the other comprising almost exclusively EpiSC-AF and EpiSC-AFI/AF cells (107/110=97% cells in the cluster) (Fig. 2F,G). Consistent with bulk RNA-seq findings, EpiSC-AFI cells expressed a higher level of ectoderm-related genes such as *Dcx*, *Slc2a2*, *Neurod1*, *Zic1*, *Sox2*, *Chat*, *Olig2* and *Fabp7* (Fig. 2G,H). Based on these observations, we hypothesised that blocking Wnt activity may have primed the bulk of the EpiSC population for enhanced ectoderm propensity.

Sustained ectoderm lineage propensity of Wnt-inhibited EpiSCs

To determine which cell populations in the epiblast the EpiSCs were developmentally equivalent to, a correlation analysis of the transcriptome by zipcode mapping was performed (Peng et al., 2016) (see Materials and Methods). The results showed that EpiSCs derived under different signalling conditions matched with different progenitor populations in the late-gastrulation epiblast (Fig. 3A): (1) EpiSC-AF cells to the anterior PS and distal epiblast (neuroectoderm and mesendoderm); (2) EpiSC-AFI cells to the anterior and lateral epiblast (pan-ectoderm), including, specifically, the distal anterior epiblast (forebrain and midbrain progenitors, Cajal et al., 2012) and the anterior PS (ectoderm and mesendoderm); and (3) EpiSC-AFI/AF cells released from Wnt inhibition reverted to posterior epiblast/anterior PS (mesendoderm).

To test the robustness of predisposition of lineage differentiation, the trajectory of differentiation of the EpiSC-derived EBs was tracked over a 4-day period *in vitro* (Fig. 3B, top panel). Results of the microfluidic RT-qPCR assay of the Cell Lineage Reporter Card (Fig. S1F) showed that EpiSC-AFI cells followed a different trajectory of differentiation from that of EpiSC-AF and EpiSC-AFI/AF cells (Fig. 3B, lower panel). At day 0, prior to differentiation, EpiSC-AFI cells displayed a higher level of expression of genes related to the three germ layers, but with a preference for the ectoderm (41% compared with 35% and 19% for mesoderm and endoderm genes, respectively) compared with EpiSC-AF cells (Fig. 3C, upper panel) and EpiSC-AFI/AF cells (Fig. S4A, left panel). By day 4 of differentiation, EpiSC-AFI cells upregulated more ectoderm marker genes (41% of the reporter genes compared with 27% and 24%) such as *Sox2*, *Neurod1*, *Fabp7*, *Zic1*, *Pou4f2* and *Dcx* (Fig. 3C, lower panel; Fig. S4A, right panel). Results of these differentiation assays supported the concept that EpiSCs derived and maintained in Wnt-inhibited condition are poised and empowered for ectoderm differentiation.

In contrast, EpiSC-AFI/AF and EpiSC-AF cells displayed similar expression of the germ layer markers at day 0 (Fig. 3D, upper panel) but, by day 4, EpiSC-AFI/AF cells expressed more mesoderm (e.g. *T*, *Comp*, *Igf2* and *Myh7*) and endoderm markers (e.g. *Foxa1*, *Hand1*, *Dpp4*, *Hnf4a* and *Gata6*) (35% and 33%, respectively) and fewer ectoderm markers (7%) (Fig. 3D, lower panel) when compared with EpiSC-AF cells. Unexpectedly, releasing the EpiSCs from Wnt inhibition (EpiSC-AFI/AF) appeared to enhance the mesendoderm propensity compared with EpiSC-AF cells.

To ascertain whether the ectoderm propensity was related to Wnt inhibition, the differentiation of EpiSC-AFI+24W cells was examined. EpiSC-AFI+24W cells followed a trajectory of differentiation that was intermediate between EpiSC-AFI and EpiSC-AF cells (Fig. S4B). Reporter card gene analysis revealed that neither day 0 nor day 4 EpiSC-AFI+24W cells showed any difference in lineage propensity from EpiSC-AF cells (Fig. S4C). Comparison of the expression of lineage markers further showed that Wnt3A treatment of EpiSC-AFI cells abolished the ectoderm propensity (Fig. S4D). Indeed, at day 0, EpiSC-AFI cells showed higher expression of markers of all three germ layers when compared with EpiSC-AFI+24W cells (Fig. S4D, upper panel), and by day 4, EpiSC-AFI cells displayed upregulated expression of ectoderm markers over EpiSC-AFI+24W cells (Fig. S4D, lower panel). Interestingly, a 24 h stimulation was able to counteract the inhibitory effect and has re-wired the lineage propensity of EpiSC-AFI.

Development (2019) 146, dev172858. doi:10.1242/dev.172858

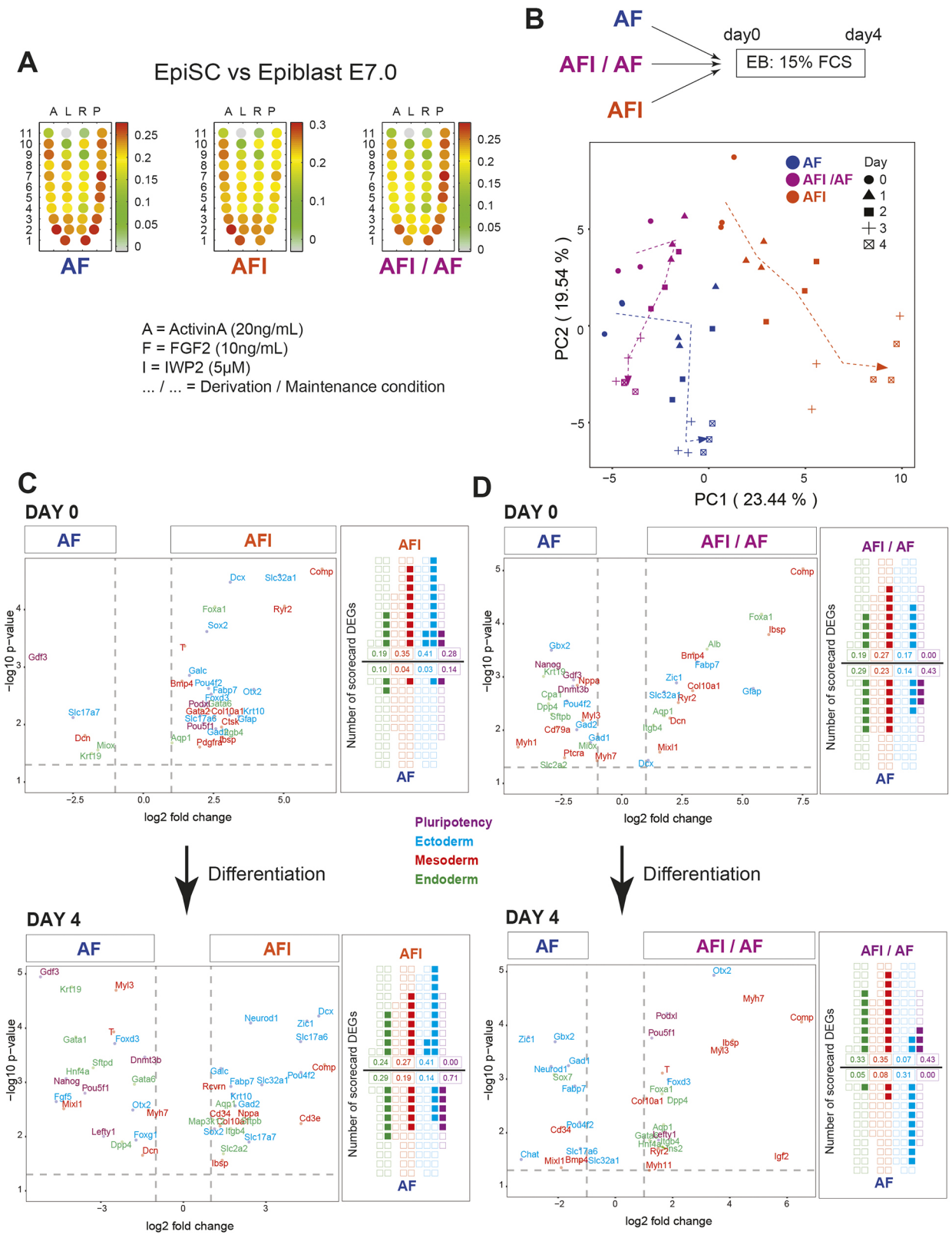

Fig. 3. See next page for legend.

In order to strengthen our findings, we collated the published dataset of other types of EpiSCs for an analysis of the DEGs (Table S6). The DEG set of rsEpiSCs (IWR1 treated) (Wu et al., 2015) (Fig. S5A) was enriched for neurogenesis development ontology but not epidermis, endoderm or mesoderm development (Fig. S5B), similar to the EpiSC-AFI cells in our study (Fig. 2D). In the IWP2-treated ESC-derived EpiSCs (ESD-EpiSC-IWP2) (Kurek et al., 2015, Fig. S5C), there was no significant enrichment

Development (2019) 146, dev172858. doi:10.1242/dev.172858

Fig. 3. Non-directed differentiation of the EpiSC-AF, AFI/AF and AFI lines. (A) The corn plots show the mapping of the EpiSC lines that were derived and maintained in different signalling conditions *in vitro* to the equivalent cell populations of known prospective fates in the E7.0 epiblast. Positions in the epiblast: 1-11, distal to proximal; A, anterior quadrant, L, left quadrant, R, right quadrant, P, posterior quadrant. Mapping was performed using the iTranscriptome online zipcode tool (see Materials and Methods) (www.picb.ac.cn/hanlab/itranscriptome/Home/). (B) Illustration of the *in vitro* differentiation assay of EBs derived from AF, AFI/AF and AFI EpiSCs. The EBs were cultured in 15% FCS-supplemented medium for 4 days. Samples were collected every day for microfluidic qPCR analysis. PCA display of the trajectory of differentiation of EBs derived from AF, AFI/AF and AFI EpiSCs from day 0 to day 4 of *in vitro* differentiation, charted by the time-course expression of lineage-related genes (Fig. S1F). EB differentiation was assessed by the expression of lineage reporter card genes and the trajectory was constructed by connecting the centroid of replicates at successive time points (samples in triplicate). Percentage in brackets indicates the variance proportion displayed by the first two axes. (C,D) Volcano plots of microfluidic qPCR data of the differentially expressed lineage markers for (C) EpiSC-AF versus EpiSC-AFI and (D) EpiSC-AF versus EpiSC-AFI/AF lines at day 0 and day 4 of *in vitro* differentiation (black arrows represent differentiation time). The *x*-axis indicates the log2 fold change between EpiSC types; the *y*-axis indicates the -log10 (*P*-value). Dashed lines indicate thresholds at fold change>2 and $P<0.05$. Scorecard summary of the volcano plot data of differentially expressed lineage markers (scorecard DEGs) with each square representing a lineage marker; filled squares indicate DEGs in the specific EpiSC type: red, mesoderm; blue, ectoderm; green, endoderm; purple, pluripotency. The number underneath each group of genes represent the proportion of genes differentially expressed for each germ layer.

of any of the four ontologies (Fig. S5D). This is likely because the EpiSCs were derived from ESCs *in vitro*, which were shown to have different molecular attributes from EpiSCs derived directly from the post-implantation epiblast (Osteil et al., 2015). Furthermore, ESD-EpiSC-IWP2 cells showed less overlap with EpiSC-AFI cells or rsEPiSCs in the profile of upregulated DEGs (Fig. S5E), suggesting that treatment with IWP2 for 48 h might not be sufficient to enhance the ectoderm propensity. A similar outcome was found in established EpiSC-AF cells that were subsequently subjected to extended IWP2 treatment (Liu et al., 2018), indicating that, once EpiSCs were established in the activin A/FGF2 condition, further modulation of Wnt activity may have no effect on the lineage propensity.

Interestingly, DEGs of EpiSC-AFI cells and rsEpiSCs showed overlap with the neurogenesis gene ontology and genes containing Lef1-binding sites in their promoter region (Fig. S5F), thus reinforcing the link between ectoderm propensity (e.g. *Dcx*) and Wnt signalling.

Wnt signalling reactivation is necessary for ectoderm differentiation

During the differentiation of EpiSC-AFI cells in high-serum content medium, the expression of *Wnt3a*, a Wnt ligand, *Lef1*, a co-activator of Wnt targets (from day 1 to day 2), and other Wnt response genes, such as *Axin2*, *Ccnd2*, *Ccnd1*, *Ntrk2*, *Sfrp2* and *Id2*, was upregulated compared with EpiSC-AFI/AF cells (Fig. 4A). In view of the enhanced expression of ectoderm genes in EpiSC-AFI cells (Fig. S4A, right panel), we hypothesised that ectoderm differentiation is promoted first by the inhibition of Wnt activity during lineage allocation followed by the reactivation of the Wnt pathway as EpiSCs exit the pluripotency state.

To test the aforementioned hypothesis, EpiSCs were cultured in serum-free conditions which favours ectoderm differentiation (Fig. 4B). EpiSC-AFI cells were also cultured in IWP2-supplemented medium to test the impact of constant inhibition of Wnt signalling on cell differentiation. As shown previously, EpiSC-AFI displayed a different trajectory of differentiation from that of the EpiSC-AF and EpiSC-AFI/AF (Fig. 4C) and upregulated more ectoderm genes relative to EpiSC-AF cells (Fig. 4D). However, EpiSC-AFI cells differentiated in the presence of IWP2 (EpiSC-AFI+IWP2, Fig. 4B) showed poor response to directed differentiation compared with EpiSC-AFI cells. EpiSC-AFI+IWP2 did not progress as far in differentiation as EpiSC-AFI cells (Fig. 4C) and showed reduced expression of ectoderm genes such as *Dcx*, *Fabp7*, *Gad1*, *Gad2*, *Slc31a1*, *Gbx2* and *Zic1*, whereas mesendoderm genes such as *Myl3*, *Igf2*, *Itgb4* and *Pdgfra* were upregulated when compared with EpiSC-AFI cells differentiated in the absence of IWP2 (Fig. 4E). We inferred that the reactivation of Wnt signalling in EpiSC-AFI cells is instrumental for ectoderm differentiation. Collectively, the findings highlighted that inhibition of Wnt activity in the self-renewing EpiSC-AFI cells poises the cells for ectoderm differentiation and enables the EpiSCs to activate the Wnt signalling pathway that promotes the differentiation of ectoderm derivatives.

Mapping the EpiSCs to the epiblast cell populations in the epiblast

To establish the developmental correlate of the EpiSCs derived from the E6.5 epiblast under different conditions, we mapped the EpiSCs to the developmental timeline of epiblast cell populations of E5.5 to E7.5 embryos (Fig. S6A, data from Liu et al., 2018). EpiSCs generated in the present study were developmentally similar to the epiblast of the E7.0 late mid-streak stage embryo (Fig. S6B). The meta-analysis of other types of EpiSC also showed that EpiSCs derived in conditions of Wnt inhibition by IWR1 (rsEpiSCs, Wu et al., 2015; EpiSC-IWR1, Liu et al., 2017) and IWP2 (ESD-EpiSC-IWP2, Kurek et al., 2015) and Wnt3A/BMP supplementation (Kurek et al., 2015) were clustered in the same PCA space that aligned with the E7.0 embryo (Fig. S6B). The meta-analysis suggests that inhibiting Wnt did not affect the developmental signature but rather poised the cells for the ectoderm lineage. The Wnt-inhibited EpiSCs remained pluripotent but displayed enhanced propensity for ectodermal differentiation.

Collectively, the activity of endogenous Wnt promotes the mesendoderm propensity of the EpiSCs, while blocking/removing Wnt activity enhances the acquisition of ectoderm propensity. The acquisition of lineage propensity by the EpiSCs under different signalling conditions therefore models the allocation of the epiblast cells to the germ layer progenitors during gastrulation and the regionalisation of progenitor cells during embryonic patterning (Fig. 5).

DISCUSSION

Wiring the lineage potency of pluripotent stem cells through priming with appropriate signalling activity provides an effective means to guide the first steps of cell differentiation and potentially enhance the efficacy of directed differentiation. EpiSCs derived under Wnt inhibition acquire a predominately ectoderm fate, suggesting that persistent repression of Wnt activity is conducive for the specification of ectoderm progenitors *in vitro*. EpiSC-AFI cells were transcriptionally equivalent to the anterior epiblast of the late gastrulation stage embryo, which is predisposed for ectoderm differentiation (Beddington, 1981, 1982; Cajal et al., 2012; Lawson and Pedersen, 1987; Tam, 1989). EpiSC-AFI cells also displayed the suppression of gene activity related to the specification and differentiation of the mesendoderm lineages (Fig. 2D). Consistent with this outcome, genome-wide transcriptome analysis of the EpiSC-AFI cells showed enrichment of DEGs for neurogenesis and depletion of those for endoderm and mesoderm differentiation.

Development (2019) 146, dev172858. doi:10.1242/dev.172858

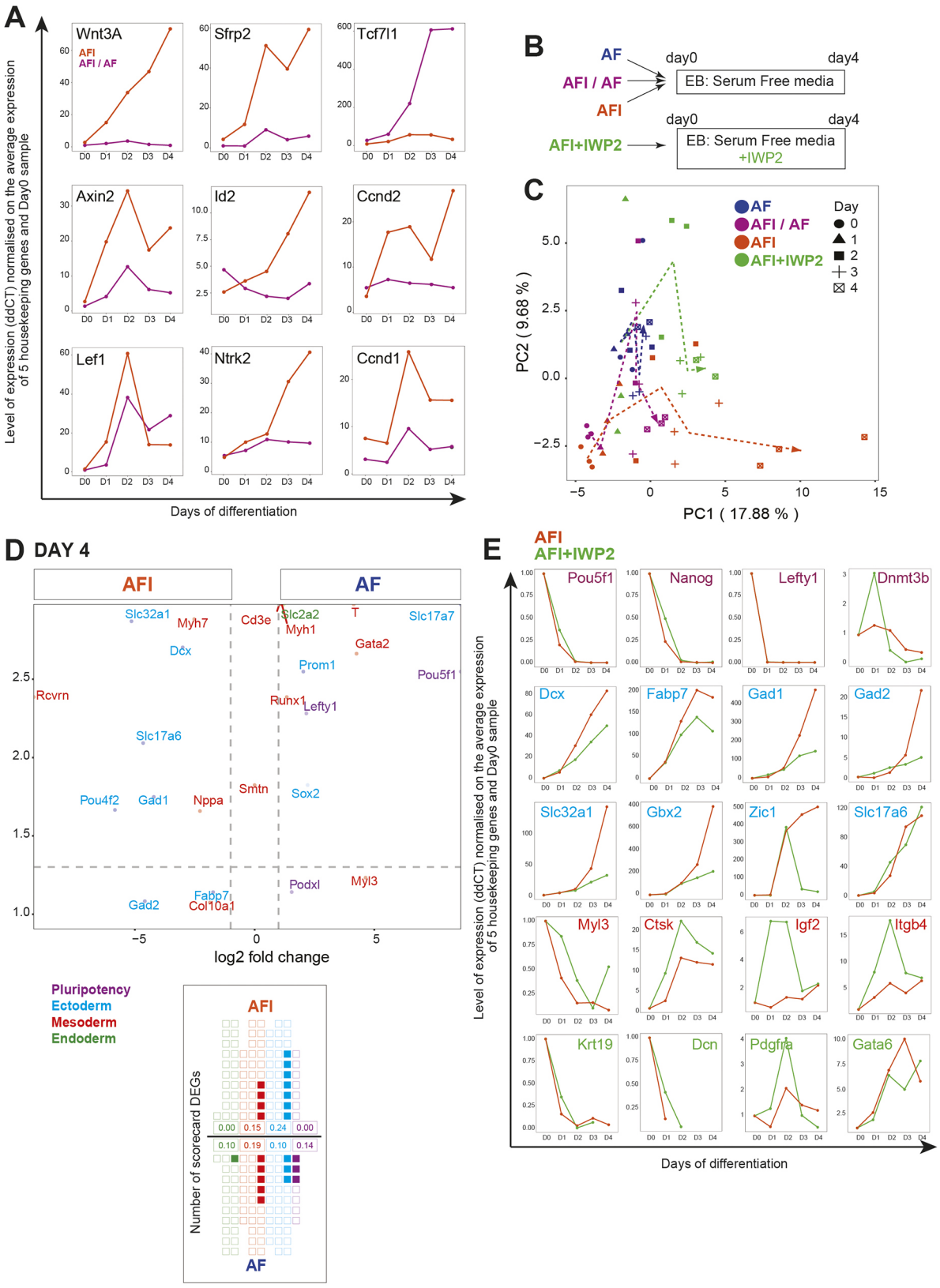

Fig. 4. See next page for legend.

A similar pattern of gene enrichment and a common set of upregulated genes of the neurogenesis ontology, which are potential Wnt target genes, were found in the EpiSCs derived in the presence of another Wnt inhibitor, IWR1 (Wu et al., 2015) (Fig. S5F). The inhibition of Wnt activity therefore primes EpiSCs for ectoderm differentiation, while suppressing their mesendoderm potency.

Of note is the faithful translation of the initial ectoderm propensity to later tissue differentiation under non-directed and

Development (2019) 146, dev172858. doi:10.1242/dev.172858

Fig. 4. Directed ectodermal differentiation of the EpiSC-AFI, AFI/AF and AF lines. (A) The expression pattern of Wnt signalling pathway target genes in EBs derived from EpiSC-AFI/AF (purple) and AFI (orange) (Fig. 3A) lines. The *x*-axis indicates days of *in vitro* differentiation; the *y*-axis indicates ddCT value of microfluidic qPCR analysis normalised to the average expression level of five housekeeping genes with the lowest expression level at day 0. (B) Protocol of directed ectoderm differentiation of EBs derived from EpiSC-AF, EpiSC-AFI/AF, EpiSC-AFI and EpiSC-AFI+24W lines. The EBs were cultured in 20% serum replacement (KOSR)-supplemented medium for 4 days. Samples were collected every day for microfluidic qPCR. (C) PCA display of the different trajectories of differentiation (tracked through the centroid of replicates) of EBs derived from EpiSC-AF, EpiSC-AFI/AF, EpiSC-AFI and EpiSC-AFI+IWP2 lines (condition where IWP2 was maintained during differentiation is in green) from day 0 to day 4 of *in vitro* differentiation. The time course of differentiation was charted by the expression of lineage reporter card genes (samples in triplicate). Percentage in brackets indicates the variance proportion displayed by the first two PC axes. (D) Volcano plot of microfluidic qPCR data of the differentially expressed lineage markers in the AFI and AF EpiSCs at day 4 of directed differentiation *in vitro*. The *x*-axis indicates the log2 fold change between EpiSC types; the y-axis indicates the -log10(*P*-value). Dashed lines indicate thresholds at $-1<\log2$ fold change<1 at $P>-\log10(0.05)=1.3$. Scorecard summary of the volcano plot data of differentially expressed lineage markers (scorecard DEGs) with each square representing a lineage marker. Filled squares indicate DEGs in the specific EpiSC type: red, mesoderm; blue, ectoderm; green, endoderm; purple, pluripotency. The number underneath each group of genes represent the proportion of genes expressed for each germ layer. (E) Time-course profiles of the expression of lineage reporter genes in EBs derived from EpiSC-AFI cells differentiated in medium without IWP2 (orange) or in the presence of IWP2 (dark green) for 4 days of *in vitro* differentiation. Lineage-related genes: ectoderm (blue), mesoderm (red), endoderm (green) and pluripotency (purple). The *x*-axis indicates days of *in vitro* differentiation; the *y*-axis indicates ddCT values of qPCR analysis normalised to the average expression level of five housekeeping genes with the lowest expression level at day 0 (samples in triplicate).

directed *in vitro* conditions. EpiSC-AFI cells followed a trajectory of differentiation that is distinct from EpiSC-AF with a significant disposition towards the ectodermal lineages (Fig. 3B, lower panel). Interestingly, withdrawing the Wnt inhibition led the cells to lose their ectoderm potency, denoting a plasticity in the cell fate commitment (Fig. 2E).

A novel insight into the mechanistic drive of EpiSCs towards ectoderm differentiation is the subsequent activation of the Wnt pathway in the differentiating EpiSC-AFI cells (Fig. 4A). EpiSC-AFI cells launch a robust activation of the Wnt pathway above that of the EpiSC-AF and EpiSC-AFI/AF cells (both being the equivalent of the posterior epiblast *in vivo* - Fig. 3A), which in turn, may drive the gene regulatory network for neurogenesis to promote neural differentiation in head morphogenesis (Fig. 4D). The unresponsiveness of EpiSC-AFI cells to directed differentiation when Wnt activity was constantly inhibited was consistent with a crucial role of launching Wnt activity for promoting neuroectoderm differentiation. An active Wnt signalling activity has been shown to drive the expansion of neural precursors from the neuromesoderm progenitor at later stage of axis development (Garriock et al., 2015). Although the mechanism of interpreting the Wnt signalling input for poising and facilitating ectoderm differentiation is yet to be fully resolved, the results of the modelling experiment infer that repression of Wnt activity is essential for the acquisition of ectoderm potency by the epiblast.

The modelling of anterior epiblast development in EpiSCs has revealed new insights into the active role of Wnt activity in the specification of anterior tissue progenitors. The EpiSC model mirrors the enhancement of ectoderm lineage potency through the repression of Wnt signalling at the inception of ectoderm progenitors in the anterior epiblast. This initial step also primes the epiblast cells for future robust activation of Wnt signalling that, in turn, drives neurogenesis of the anterior epiblast. In the *Dkk1* mutant embryo, the loss of antagonistic activity results in posteriorisation of the anterior epiblast and loss of ectoderm potency that underpins the failure of neuroectoderm differentiation and loss of brain structures. Enhancing Wnt activity promotes the formation of posterior structures while missing the crucial step of suppressing Wnt activity may be associated with the absence of anterior (head) tissues in the ESC-derived gastruloid (Beccari et al., 2018). The regionalised modulation of Wnt activity during gastrulation is therefore crucial for the allocation of anterior epiblast cells to the ectoderm over the mesendoderm lineage, a key requisite step in embryonic patterning and the formation of the embryonic head.

MATERIALS AND METHODS

Derivation and maintenance of the EpiSC lines

All the animals in our study were used in compliance with the Australian Code for the Care and Use of Animals for Scientific Purposes, 8th Edition 2013, the Animal Research Act 1985 and the Animal Research Regulation 2010. The Children's Medical Research Institute Animal Ethics Committee is reviewing each project before approval. All embryos were collected from the 129 strain and 8-week-old pregnant female.

Irradiated mouse embryonic fibroblasts (MEFs) were seeded 1 day prior to splitting EpiSC (Osteil et al., 2015). EpiSC lines were derived from the epiblast of early-streak stage 129 strain mouse embryo, as previously described (Kojima et al., 2014; Osteil et al., 2015). Briefly, dissected epiblast were maintained on gelatine 0.1% (Sigma, G9391) and inactivated mouse embryonic fibroblasts (MEF) in EpiSC culture medium consisting of Knockout-DMEM (ThermoFisher Scientific, 10829-018), Knockout Serum Replacement (ThermoFisher Scientific, 20%, 10828-028), Non-Essential Amino Acid (ThermoFisher Scientific, 1×, 11140-050), GlutaMAX (ThermoFisher Scientific, 1×, 35050-061), penicillin-streptomycin (ThermoFisher Scientific, 50 Units/ml and 50 µg/ml, 15070-063) and β-mercaptoethanol (Sigma, M3148). Media were supplemented with recombinant human FGF2 (10 ng/ml, R&D systems, 233-FB), and recombinant human/mouse/rat activin A (20 ng/ml, R&D systems, 338-AC) and IWP2 (5 µM, Sigma, I0536).

Upon reaching confluency, EpiSC colonies were detached from the MEF with collagenase IV (ThermoFisher Scientific, 17104-019), reconstituted in EpiSC culture medium and dissociated to single cells using TrypLE Select (ThermoFisher Scientific, 12563-011). To enhance cell viability, dissociated EpiSC were plated down in their respective media supplemented with ROCK inhibitor Y27632 dihydrochloride (10 ng/ml, Tocris, 1254) for 24 h.

EpiSC-AF lines were derived and maintained in medium supplemented with FGF2 and activin A, and EpiSC-AFI cells were derived and maintained in medium further supplemented with IWP2. Established EpiSC-AFI lines were converted to: (1) EpiSC-AFI/AF lines by culturing in FGF2- and activin A-supplemented medium without IWP2 [EpiSC-AFI/AF cells were maintained for over six passages before use for experimentation.]; and (2) EpiSC-AFI+24W cells by culturing with Wnt3A for 24 h (100 ng/ml, R&D, 1324-WN-010). [*Dkk1*-null mutant EpiSC lines (EpiSC-AF$^{Dkk1-/-}$) were derived and maintained in the culture medium containing FGF2 and activin A.]

Analysis of the expression of pluripotent and signalling markers in EpiSC

EpiSCs were cultured on 14 mm circular glass coverslips in 24-well tissue culture plates, pre-seeded with mouse embryonic fibroblasts (MEFs). EpiSCs were plated on the MEFs at a density of 1×10^5 cells per well. Three replicate wells were set up for each experimental condition. After 2 days of *in vitro* culture, cell samples were fixed and permeabilised in 4% paraformaldehyde (PFA) supplemented with 0.3% Triton X100 for 5 min and subsequently in 4% PFA for an additional 10 min. Fixed cells were rinsed in PBS (3×5 min) and blocked in CAS-Block (ThermoFisher Scientific, 00-8120) for 1 h at room temperature.

Immunohistochemistry was performed using primary antibodies according to Table S7. Fixed cells on glass coverslips were incubated

Development (2019) 146, dev172858. doi:10.1242/dev.172858

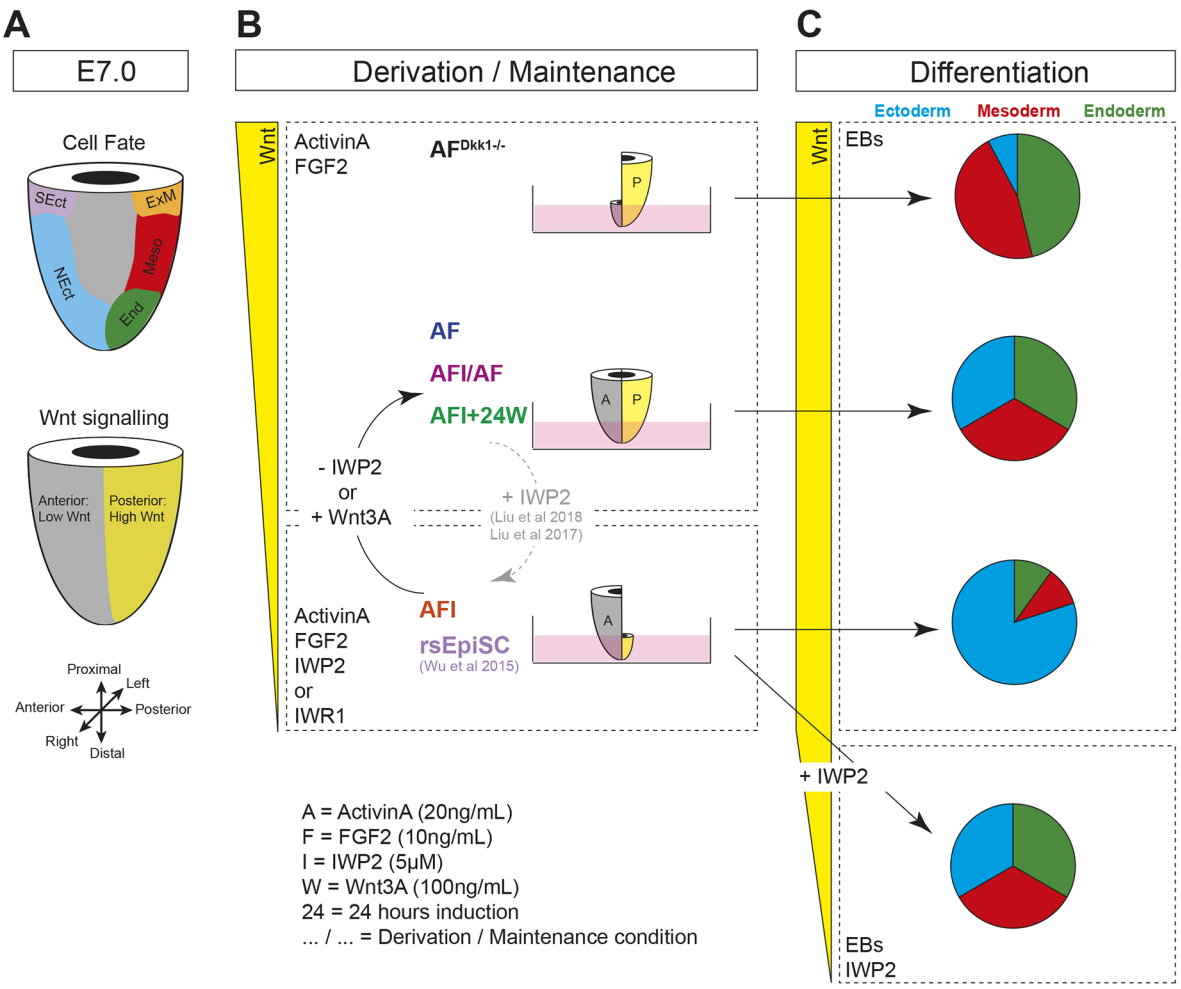

Fig. 5. Modelling the cell fate acquisition in the epiblast by using EpiSCs. Summary of the findings. (A) Prior to gastrulation, the posterior and the anterior epiblast are endowed with different Wnt activity: low in anterior tissues (grey) and high in the posterior tissues (yellow) (bottom). Epiblast cells in the primitive streak (in the posterior epiblast) are allocated to the mesendoderm (top). (B) EpiSCs isolated from *Dkk1*-null mutant embryos differentiate predominately into mesendodermal derivatives (top) when compared with conventional EpiSC-AF. EpiSCs derived and maintained in the presence of Wnt inhibition (EpiSC-AFI or rsEpiSCs) displayed enhanced propensity for the ectoderm lineage that is characteristic of the anterior epiblast cells and differentiated preferentially to ectoderm derivative. Withdrawing the inhibition or providing exogenous Wnt activity diminishes the ectoderm propensity (AFI/AF and AFI+24W) and reverts the lineage profile to that of the conventional EpiSCs [derived and maintained in activin A and FGF2 (AF)]. Reactivation of Wnt activity during the differentiation (yellow gradient box) of the Wnt-inhibited EpiSCs enhanced ectoderm differentiation (bottom pie chart). (C) Pie charts show the outcome of differentiation into ectoderm, mesoderm and endoderm derivatives in the embryoid bodies (EBs). Constant inhibition of Wnt activity impacts adversely on the differentiation of the EpiSCs into ectoderm derivatives.

overnight at 4°C with antibodies that were diluted in CAS-Block. After rinsing with PBS for 3×6 min, the cell samples were incubated in darkness at room temperature for 1 h with secondary antibodies (Table S7) and counterstained with DAPI for 10 min at room temperature. The coverslips were mounted on glass slides using Fluromount G mounting media (Southern Biotech, 0100-01). Fluorescence images were captured using a Zeiss AxioCam MRc camera on an LMS 880 microscope (Zeiss). Fluorescent signal of nuclear content was captured with threshold setting for imaging only the DAPI-stained nucleus and data were analysed using the Fiji image analytic tools. Number of nuclei analysed is indicated for each cell type. *P*-values were estimated by Mann-Whitney-Wilcox non-parametric test: ***P<0.001; **P<0.01; *P<0.05; ns, non-significant.

Assessing the level of canonical Wnt activity in EpiSCs cultured in different conditions using β-galactosidase staining

EpiSC were seeded over MEF at a density of 2×10^5 cells per well in 12-well plates and cultured in triplicate. After 2 days in culture, cells were rinsed twice in PBS prior to and after being fixed in 4% PFA for 5 min. Fixed cells were then incubated at 37°C overnight in the dark, in X-gal solution [2 mM $MgCl_2$, 5 mM potassium ferricyanide (Sigma, P-3667), 5 mM potassium ferrocyanide (Sigma, P-3289), 1 mg/ml X-gal (Quantum Scientific, 00-0190), 0.1% Tween20 in PBS]. Cells were then rinsed in PBS and analysed on a luminometer.

Differentiation assay

Differentiation was induced by culturing the EpiSCs in serum-supplemented medium. Upon reaching 90% confluency, EpiSC were passaged and 2×10^6 EpiSC were collected as a cell pellet for gene expression analysis (day 0). EpiSCs (5×10^5 cells) from each treatment group were seeded into each well of a 6-well ultra low-adhesion plate (Corning, 3471) with EB medium supplemented with ROCK-inhibitor [Knock-Out DMEM (ThermoFisher Scientific, 10829-018)]. For non-directed differentiation, the medium was supplemented with FCS (15%, Serana, S-FBS-AU-015). For directed differentiation, KnockOut Serum Replacement (20%, ThermoFisher Scientific, 11140-050) was used in the place of FBS. Both media contained 1% Non-Essential Amino Acid (1×, ThermoFisher Scientific, 11140-050), 1% GlutaMAX (1×, ThermoFisher Scientific, 35050-061), 1% penicillin-streptomycin (50 Units/ml and 50 µg/ml, ThermoFisher Scientific, 15070-063) and 0.1 mM β-mercaptoethanol (Sigma, M3148)]. Newly formed EBs were transferred

Development (2019) 146, dev172858. doi:10.1242/dev.172858

to 10 cm bacterial-grade petri dishes with EB medium without ROCK-inhibitor 24 h later. EBs were re-fed every 2 days and collected daily from days 1 to 4, pelleted, snap-frozen in liquid nitrogen and stored at −80°C.

Gene expression analysis by microfluidic qRT-PCR in bulk population and single-cell

RNA was extracted from cell samples with the ISOLATE II RNA Mini Kit (Bioline, BIO-52075), then was reverse transcribed to cDNA using reagents from the RT2 Microfluidics qPCR Reagent System kit (Qiagen, 330431), as per the manufacturer's protocol. cDNAs were pre-amplified using the RT2 PreAMP Pathway Primer Mix for amplification of Cell Lineage marker genes (Qiagen, PAMM-508Z) and Wnt signalling target genes (Qiagen, PAMM-243Z). qPCR was then performed on the sets of pre-amplified cDNA using the above primer sets. Each set of primers resulted in a different dataset that was analysed independently.

High-throughput gene expression analysis (BioMark HD System, Fluidigm) was performed on EpiSCs to assess the expression profile of Wnt target genes and cell lineage gene markers prior to and throughout the 4-day differentiation time course. Raw data were extracted using the Fluidigm Real-Time PCR Analysis Software and subsequent analysis was performed in R software. Ct values flagged as undetermined or greater than the threshold (Ct>24) were set to NA (missing values). Samples with a measurement for only one housekeeping gene or samples with measurements for <30 genes were excluded from further analysis. Genes where over 30 samples had a measurement of NA were also excluded from further analysis. Delta Ct was calculated by subtracting the average expression of five housekeeping genes (*Gapdh*, *B2m*, *Gusb*, *Hsp90aa1* and *Actb*) from the sample gene expression. Differential gene expression analysis was performed using an ANOVA test followed by Tukey's 'Honest Significant Difference' method.

Single-cell qRT-PCR sample preparation and data analysis

The single-cell Auto prep system from Fluidigm was used as per the manufacturer's protocol. Briefly, cells were passaged as usual and ∼200 cells were loaded on the C1 Array IFC (Fluidigm, 10-17 µm, 100-5749). Lysis, reverse transcription and specific target amplification were performed using the Cells-to-Ct kit (Ambion, 4458237). Pre-amplification were performed using primer set for 'Cell Lineage marker' (Qiagen, PBM-508ZH). cDNAs were collected and RT-qPCR were carried out using 96.96 Dynamic Arrays on a BioMark system (Fluidigm).

Raw data pre-processing was performed following the same step as above. For differential gene expression analysis, the Kruskal–Wallis test and the Dunn post-hoc test, multiple test correction was performed using the FDR method, with a significance threshold of *P*.adjust<0.05.

Microarray sample preparation

Fifteen *Dkk1*$^{+/+}$ embryos and 15 *Dkk1*$^{-/-}$ sibling embryos (129×C57BL/6 background) were collected at E7.75 early-bud/early-headfold stage. The embryos were bisected longitudinally into anterior and posterior halves that were snap-frozen independently. The yolk sac of each embryo was also collected and used for genotyping. Samples of the same genotype were pooled in three independent pools of five half-embryos each. RNA was extracted using RNeasy MicroKit (Qiagen,74004) for each pool (approximately 250 ng total RNA per pool) and used for microarray analysis using Illumina Mouse WG-6 v2 Expression Beadchip at the Australian Genome Research Facility (AGRF).

Data analysis was performed in R using beadarray and illuminaMousev2.db libraries. The raw expression values were quantile normalised and log2 transformed. Probes annotated as of bad quality, according to illumina Mousev2 PROBEQUALITY, were removed. The maximum expression value was used when multiple probes corresponded to a single gene were analysed.

RNA-seq sample preparation, sequencing design and data analysis

RNA was extracted from EpiSCs in triplicate (at three different passages: 4, 6 and 7 after acclimatisation in maintenance conditions). RNA was extracted from cell samples with the ISOLATE II RNA Mini Kit (Bioline, BIO-52075) and RNA quality was verified using a Bioanalyzer (Agilent Technologies). The 12 samples RNA Integrity Number was 10, confirming the quality of the RNA and suitability for RNA-Seq analysis. Library preparation was performed with 20 µl of total RNA at 100 ng/µl using the TruSeq Stranded mRNA Sample preparation protocol. Sequencing was performed using 50 bp single-end reads to a depth of 20 million reads per sample.

Raw reads from published dataset and from newly generated data were extracted and aligned using Salmon program (Patro et al., 2017) using reference transcriptome M17 (05/04/2018) from Gencode (www.gencodegenes.org/), which converts the raw reads into transcripts per million (TPM). Counts were imported to R using tximport (Soneson et al., 2016). Then, transcripts with count value of 0 across all conditions were removed from the analysis. We performed normalisation of the TPM across the different samples using DESEq2 (Love et al., 2014) and negative binomial transformation of the data per sample was performed by using the EdgeR package (Robinson et al., 2009). DEGs were extracted using DESeq2 and plotted accordingly as a volcano plot (Log2 Fold Change versus Log10 negative *P* value). Barcoded plots [Limma package (Ritchie et al., 2015)] were generated using the qusage package (Yaari et al., 2013) with the Gene Ontology database 'c5.bp.v6.1.symbols.gmt' (software.broadinstitute.org/gsea/msigdb/collections.jsp#C2).

When we only had access to a list of genes lists from the microarray (e.g. Fig. 1C), gene ontology enrichment analysis was performed using TOPPGene (Chen et al., 2009b) for biological process on the mouse species. PCA analysis as performed using the pcrcomp function ['stats' library v3.4.1 (Venables and Ripley, 2002)] and R. Hierarchical clustering was performed using the heatmap function with the 'Minkowski' method.

Western blot

Sample preparation

Epiblast stem cells were resuspended in 50 µl of RIPA buffer consisting of 1% Ipegal CA-630, 0.5% sodium deoxycholate, 0.1% SDS, 1 mM DTT, 1× Complete Protease Inhibitor Cocktail (Sigma-Aldrich, 11836145001), 1× PhosSTOP EASYPack (Roche, 04906845001) phosphatase inhibitor and 1.5% Triton X-100 in Dulbecco's phosphate-buffered saline. Samples were vortexed until homogenised and rotated at 4°C for 45 min. Samples were centrifuged for at 15,000 ***g*** for 10 min at 4°C and the supernatant containing soluble proteins was collected.

Protein concentration was determined using Direct Detect Assay free cards (Merck, DDAC00010-GR). 2 µl of sample was pipetted on each membrane panel and concentration was determined using a Direct Detect Spectrometer (Merck, DDHW00010-WW) with RIPA buffer used as a blank. Samples were made up to a concentration of 0.5 µg/µl using Milli-Q Ultrapure Water (Merck, ZIQ7000T0). 5× SDS loading dye [5% β-mercaptoethanol, 0.02% Bromophenol Blue, 30% glycerol, 10% sodium dodecyl sulfate, 250 mM Tris-Cl (pH 6.8)] was then added to the samples. Samples were heat inactivated at 90°C for 10 min.

Protein separation and transfer

A Novex Nu-PAGE pre-cast 4-12% gradient Bis-Tris 12-well gel (Life Technologies, NP0322BOX) was loaded in an XCell SureLock Novex Mini-gel electrophoresis chamber (Life Technologies, EI0001). Running buffer (1×) was made from 20× stock (50 mM MES, 50 mM Tris-Base, 0.1% SDS and 1 mM EDTA) with MilliQ-Ultrapure Water and added to the electrophoresis chamber. Protein sample (15 µl) was run against 9 µl Novex Sharp Pre-stained Protein Standard (Invitrogen, LC5800) for 60 min at 200V. Gels were transferred to Whatman Optitran BA-S 83 0.2 µm nitrocellulose membranes (Sigma-Aldrich, 10439380) sandwiched between 3MM Chr Whatman paper (Sigma-Aldrich, 3030-917). The transfer was run in a Mini Trans-Blot Electrophoretic Cell (BioRad, 170-3930) in 1× Towbin transfer buffer made from a 5× stock (50 mM Tris-base and 200 mM glycine) with 10% methanol for 60 min at 90V at 4°C.

Antibody application

Membranes were washed in 1× PBST made from 10× PBS stock (PBS tablets, MP Biomedicals, 2810305) and 0.001% Tween20 (Sigma-Aldrich, 9005-64-5). Membranes were blocked in blocking agent as applicable for antibody (Table S7) for 60 min before primary antibodies were applied overnight while rocking at 4°C. The following day, membranes were washed with PBST and secondary antibodies were applied for 60 min at room

Development (2019) 146, dev172858. doi:10.1242/dev.172858

temperature. Antibodies were stored with 2% sodium azide at 4°C for further use. Membranes were revealed using SuperSignal West Pico PLUS Chemiluminescent Substrate (ThermoFisher, 34580) according to the manufacturer's instructions. Membranes were imaged with a Fujifilm LAS4000 Luminescence Imager.

Meta-analysis with embryonic fragments and mapping to the E7.0 embryo

All samples were first normalised using binomial normalisation. Then the developmental trajectory of the epiblast of E5.0-E7.5 embryo fragment (Liu et al., 2018) was defined by the stage-specific expression of the top and bottom 200 differentially expressed time-related genes. These 400 genes were used to plot the PCA on Fig. S6B.

Zipcode mapping of epiblast against embryo

According to the previous analysis, our data were mapped against the E7.0 embryo using the iTranscriptome zipcode mapping tool online (www.picb.ac.cn/hanlab/itranscriptome/Home/). Zipcode analysis was performed by extracting 158 genes that constitute the minimal set of genes to positively discriminate the 42 regions in the E7.0 epiblast, i.e. they are a set of domain-specific signature genes. Then the data were submitted to a support vector machine (SVM) for training purposes and validated using two other embryos. By extracting expression value of the 158 genes it is now possible to pinpoint the region with the closest transcriptomic signature to a given sample (Peng et al., 2016).

Acknowledgement

We thank Scott Page (ACRF Telomere Analysis Centre) for assistance with imaging analysis. The ACRF Telomere Analysis Centre is supported by the Australian Cancer Research Foundation.

Competing interests

The authors declare no competing or financial interests.

Author contributions

Conceptualization: P.O., H.N.G., X.F., N.F., P.P.L.T.; Methodology: P.O., J.B.S., H.N.G., E.E.W., X.F., P.-L.K., G.P., N.S., H.K., N.F.; Validation: P.O., J.B.S.; Formal analysis: P.O., E.E.W., G.P.; Resources: P.O.; Data curation: E.E.W.; Writing - original draft: P.O., H.K., P.P.L.T.; Writing - review & editing: P.O., X.F., N.S., N.F., P.P.L.T.; Visualization: P.O.; Supervision: P.O., J.-D.J.H., N.J., P.P.L.T.; Project administration: P.O., P.P.L.T.; Funding acquisition: P.P.L.T.

Funding

Our work was supported by the National Health and Medical Research Council of Australia (632776), the Australian Research Council (DP 160103651) and Mr James Fairfax. P.O. was supported by the Fondation pour la Recherche Médicale (FRM SPE20140129375). P.P.L.T. is an National Health and Medical Research Council Senior Principal Research Fellow (1110751).

Data availability

The RNAseq and microarray data have been deposited in GEO under accession number GSE103369.

Supplementary information

Supplementary information available online at
http://dev.biologists.org/lookup/doi/10.1242/dev.172858.supplemental

References

Arkell, R. M. and Tam, P. P. L. (2012). Initiating head development in mouse embryos: integrating signalling and transcriptional activity. *Open Biol.* **2**, 120030.

Beccari, L., Moris, N., Girgin, M., Turner, D. A., Baillie-Johnson, P., Cossy, A.-C., Lutolf, M. P., Duboule, D. and Arias, A. M. (2018). Multi-axial self-organization properties of mouse embryonic stem cells into gastruloids. *Nature* **562**, 272-276.

Beddington, S. P. (1981). An autoradiographic analysis of the potency of embryonic ectoderm in the 8th day postimplantation mouse embryo. *J. Embryol. Exp. Morph.* **64**, 87-104.

Beddington, R. S. (1982). An autoradiographic analysis of tissue potency in different regions of the embryonic ectoderm during gastrulation in the mouse. *J. Embryol. Exp. Morph.* **69**, 265-285.

Blauwkamp, T. A., Nigam, S., Ardehali, R., Weissman, I. L. and Nusse, R. (2012). Endogenous Wnt signalling in human embryonic stem cells generates an equilibrium of distinct lineage-specified progenitors. *Nat. Commun.* **3**, 1070.

Brons, I. G. M., Smithers, L. E., Trotter, M. W. B., Rugg-Gunn, P., Sun, B., Chuva de Sousa Lopes, S. M., Howlett, S. K., Clarkson, A., Ahrlund-Richter, L., Pedersen, R. A. et al. (2007). Derivation of pluripotent epiblast stem cells from mammalian embryos. *Nature* **448**, 191-195.

Cajal, M., Lawson, K. A., Hill, B., Moreau, A., Rao, J., Ross, A., Collignon, J. and Camus, A. (2012). Clonal and molecular analysis of the prospective anterior neural boundary in the mouse embryo. *Development* **139**, 423-436.

Chen, B., Dodge, M. E., Tang, W., Lu, J., Ma, Z., Fan, C.-W., Wei, S., Hao, W., Kilgore, J., Williams, N. S. et al. (2009a). Small molecule-mediated disruption of Wnt-dependent signaling in tissue regeneration and cancer. *Nat. Chem. Biol.* **5**, 100-107.

Chen, J., Bardes, E. E., Aronow, B. J. and Jegga, A. G. (2009b). ToppGene Suite for gene list enrichment analysis and candidate gene prioritization. *Nucleic Acids Res.* **37**, 305-311.

Cui, G., Suo, S., Wang, R., Qian, Y., Han, J. D. J., Peng, G., Tam, P. P. L. and Jing, N. (2018). Mouse gastrulation: attributes of transcription factor regulatory network for epiblast patterning. *Dev. Growth Differ.* **60**, 463-472.

Durston, A. J. (2015). Time, space and the vertebrate body axis. *Semin. Cell Dev. Biol.* **42**, 66-77.

Engert, S., Burtscher, I., Liao, W. P., Dulev, S., Schotta, G. and Lickert, H. (2013). Wnt/β-catenin signalling regulates Sox17 expression and is essential for organizer and endoderm formation in the mouse. *Development* **140**, 3128-3138.

Eroshkin, F. M., Nesterenko, A. M., Borodulin, A. V., Martynova, N. Y., Ermakova, G. V., Gyoeva, F. K., Orlov, E. E., Belogurov, A. A., Lukyanov, K. A., Bayramov, A. V. et al. (2016). Noggin4 is a long-range inhibitor of Wnt8 signalling that regulates head development in Xenopus laevis. *Sci. Rep.* **6**, 23049.

Fossat, N., Jones, V., Khoo, P.-L., Bogani, D., Hardy, A., Steiner, K., Mukhopadhyay, M., Westphal, H., Nolan, P. M., Arkell, R. et al. (2011). Stringent requirement of a proper level of canonical WNT signalling activity for head formation in mouse embryo. *Development* **138**, 667-676.

Fossat, N., Jones, V., Garcia-Garcia, M. J. and Tam, P. P. L. (2012). Modulation of WNT signaling activity is key to the formation of the embryonic head. *Cell Cycle* **11**, 26-32.

Fossat, N., Ip, C. K., Jones, V. J., Studdert, J. B., Khoo, P.-L., Lewis, S. L., Power, M., Tourle, K., Loebel, D. A. F., Kwan, K. M. et al. (2015). Context-specific function of the LIM homeobox 1 transcription factor in head formation of the mouse embryo. *Development* **142**, 2069-2079.

Garriock, R. J., Chalamalasetty, R. B., Canizales, L. C., Lewandoski, M., Kennedy, M. W. and Yamaguchi, T. P. (2015). Lineage tracing of neuromesodermal progenitors reveals novel Wnt-dependent roles in trunk progenitor cell maintenance and differentiation. *Development* **142**, 1628-1638.

Glinka, A., Wu, W., Delius, H., Monaghan, A. P., Blumenstock, C. and Niehrs, C. (1998). Dickkopf-1 is a member of a new family of secreted proteins and functions in head induction. *Nature* **391**, 357-362.

Hikasa, H. and Sokol, S. Y. (2013). Wnt signaling in vertebrate axis specification. *Cold Spring Harbor Perspect. Biol.* **5**, a007955.

Hikasa, H., Ezan, J., Itoh, K., Li, X., Klymkowsky, M. W. and Sokol, S. Y. (2010). Regulation of TCF3 by Wnt-dependent phosphorylation during vertebrate axis specification. *Dev. Cell* **19**, 521-532.

Ip, C. K., Fossat, N., Jones, V., Lamonerie, T. and Tam, P. P. L. (2014). Head formation: OTX2 regulates Dkk1 and Lhx1 activity in the anterior mesendoderm. *Development* **141**, 3859-3867.

Kazanskaya, O., Glinka, A. and Niehrs, C. (2000). The role of Xenopus dickkopf1 in prechordal plate specification and neural patterning. *Development* **127**, 4981-4992.

Kiecker, C. and Niehrs, C. (2001). A morphogen gradient of Wnt/beta-catenin signalling regulates anteroposterior neural patterning in Xenopus. *Development* **128**, 4189-4201.

Kim, S.-H., Shin, J., Park, H.-C., Yeo, S.-Y., Hong, S.-K., Han, S., Rhee, M., Kim, C.-H., Chitnis, A. B. and Huh, T.-L. (2002). Specification of an anterior neuroectoderm patterning by Frizzled8a-mediated Wnt8b signalling during late gastrulation in zebrafish. *Development* **129**, 4443-4455.

Kojima, Y., Kaufman-Francis, K., Studdert, J. B., Steiner, K. A., Power, M. D., Loebel, D. A. F., Jones, V., Hor, A., de Alencastro, G., Logan, G. J. et al. (2014). The transcriptional and functional properties of mouse epiblast stem cells resemble the anterior primitive streak. *Cell Stem Cell* **14**, 107-120.

Krupnik, V. E., Sharp, J. D., Jiang, C., Robison, K., Chickering, T. W., Amaravadi, L., Brown, D. E., Guyot, D., Mays, G., Leiby, K. et al. (1999). Functional and structural diversity of the human Dickkopf gene family. *Gene* **238**, 301-313.

Kurek, D., Neagu, A., Tastemel, M., Tüysüz, N., Lehmann, J., van de Werken, H. J. G., Philipsen, S., van der Linden, R., Maas, A., van Ijcken, W. F. J. et al. (2015). Endogenous WNT signals mediate BMP-induced and spontaneous differentiation of epiblast stem cells and human embryonic stem cells. *Stem Cell Rep.* **4**, 114-128.

Lawson, K. A. and Pedersen, R. A. (1987). Cell fate, morphogenetic movement and population kinetics of embryonic endoderm at the time of germ layer formation in the mouse. *Development* **101**, 627-652.

Lewis, S. L., Khoo, P.-L., De Young, R. A., Steiner, K., Wilcock, C., Mukhopadhyay, M., Westphal, H., Jamieson, R. V., Robb, L. and Tam,

P. P. L. (2008). Dkk1 and Wnt3 interact to control head morphogenesis in the mouse. *Development* **135**, 1791-1801.
Liu, K., Sun, Y., Liu, D. and Ye, S. (2017). Inhibition of Wnt/β-catenin signaling by IWR1 induces expression of Foxd3 to promote mouse epiblast stem cell self-renewal. *Biochem. Biophys. Res. Commun.* **490**, 616-622.
Liu, C., Wang, R., He, Z., Osteil, P., Wilkie, E., Yang, X., Chen, J., Cui, G., Guo, W., Chen, Y. et al. (2018). Suppressing nodal signaling activity predisposes ectodermal differentiation of epiblast stem cells. *Stem Cell Rep.* **11**, 1-15.
Love, M. I., Huber, W. and Anders, S. (2014). Moderated estimation of fold change and dispersion for RNA-seq data with DESeq2. *Genome Biol.* **15**, 550, 1-521.
Mao, B., Wu, W., Davidson, G., Marhold, J., Li, M., Mechler, B. M., Delius, H., Hoppe, D., Stannek, P., Walter, C. et al. (2002). Kremen proteins are Dickkopf receptors that regulate Wnt/beta-catenin signalling. *Nature* **417**, 664-667.
Maretto, S., Cordenonsi, M., Dupont, S., Braghetta, P., Broccoli, V., Hassan, A. B., Volpin, D., Bressan, G. M. and Piccolo, S. (2003). Mapping Wnt/beta-catenin signaling during mouse development and in colorectal tumors. *Proc. Natl. Acad. Sci. USA* **100**, 3299-3304.
Mukhopadhyay, M., Shtrom, S., Rodriguez-Esteban, C., Chen, L., Tsukui, T., Gomer, L., Dorward, D. W., Glinka, A., Grinberg, A., Huang, S.-P. et al. (2001). Dickkopf1 is required for embryonic head induction and limb morphogenesis in the mouse. *Dev. Cell* **1**, 423-434.
Nakamura, T., Nakamura, T. and Matsumoto, K. (2008). The functions and possible significance of Kremen as the gatekeeper of Wnt signalling in development and pathology. *J. Cell. Mol. Med.* **12**, 391-408.
Osteil, P., Studdert, J., Wilkie, E., Fossat, N. and Tam, P. P. L. (2015). Generation of genome-edited mouse epiblast stem cells via a detour through ES cell-chimeras. *Differentiation* **91**, 119-125.
Patro, R., Duggal, G., Love, M. I., Irizarry, R. A. and Kingsford, C. (2017). Salmon provides fast and bias-aware quantification of transcript expression. *Nat. Methods* **14**, 417-419.
Pearce, J. J. H., Penny, G. and Rossant, J. (1999). A mouse cerberus/Dan-related gene family. *Dev. Biol.* **209**, 98-110.
Peng, G., Suo, S., Chen, J., Chen, W., Liu, C., Yu, F., Wang, R., Chen, S., Sun, N., Cui, G. et al. (2016). Spatial transcriptome for the molecular annotation of lineage fates and cell identity in mid-gastrula mouse embryo. *Dev. Cell* **36**, 681-697.
Petersen, C. P. and Reddien, P. W. (2009). Wnt signaling and the polarity of the primary body axis. *Cell* **139**, 1056-1068.
Pfister, S., Steiner, K. A. and Tam, P. P. L. (2007). Gene expression pattern and progression of embryogenesis in the immediate post-implantation period of mouse development. *Gene Expr. Patterns* **7**, 558-573.
Ritchie, M. E., Phipson, B., Wu, D., Hu, Y., Law, C. W., Shi, W. and Smyth, G. K. (2015). Limma powers differential expression analyses for RNA-sequencing and microarray studies. *Nucleic Acids Res.* **43**, e47.
Robertson, E. J., Norris, D. P., Brennan, J. and Bikoff, E. K. (2003). Control of early anterior-posterior patterning in the mouse embryo by TGF-beta signalling. *Philos. Trans. R. Soc. Lond. B Biol. Sci.* **358**, 1351-1357.
Robinson, M. D., McCarthy, D. J. and Smyth, G. K. (2009). edgeR: a Bioconductor package for differential expression analysis of digital gene expression data. *Bioinformatics* **26**, 139-140.
Semënov, M. V., Tamai, K., Brott, B. K., Kühl, M., Sokol, S. and He, X. (2001). Head inducer dickkopf-1 is a ligand for Wnt coreceptor LRP6. *Curr. Biol.* **11**, 951-961.
Soneson, C., Love, M. I. and Robinson, M. D. (2016). Differential analyses for RNA-seq: transcript-level estimates improve gene-level inferences. *F1000Research* **4**, 1521.
Sugimoto, M., Kondo, M., Koga, Y., Shiura, H., Ikeda, R., Hirose, M., Ogura, A., Murakami, A., Yoshiki, A., Chuva de Sousa Lopes, S. M. et al. (2015). A simple and robust method for establishing homogeneous mouse epiblast stem cell lines by Wnt inhibition. *Stem Cell Rep.* **4**, 744-757.
Sumi, T., Oki, S., Kitajima, K. and Meno, C. (2013). Epiblast ground state is controlled by canonical Wnt/β-catenin signaling in the postimplantation mouse embryo and epiblast stem cells. *PLoS ONE* **8**, e63378.
Takata, N., Sakakura, E., Eiraku, M., Kasukawa, T. and Sasai, Y. (2017). Self-patterning of rostral-caudal neuroectoderm requires dual role of Fgf signaling for localized Wnt antagonism. *Nat. Commun.* **8**, 1-15.
Tam, P. P. (1989). Regionalisation of the mouse embryonic ectoderm: allocation of prospective ectodermal tissues during gastrulation. *Development* **107**, 55-67.
Tesar, P. J., Chenoweth, J. G., Brook, F. A., Davies, T. J., Evans, E. P., Mack, D. L., Gardner, R. L. and McKay, R. D. G. (2007). New cell lines from mouse epiblast share defining features with human embryonic stem cells. *Nature* **448**, 196-199.
Venables, W. N. and Ripley, B. D. (2002). *Modern applied statistics with S*, 4rd edn. New York, NY: Springer New York.
Wu, J., Okamura, D., Li, M., Suzuki, K., Luo, C., Ma, L., He, Y., Li, Z., Benner, C., Tamura, I. et al. (2015). An alternative pluripotent state confers interspecies chimaeric competency. *Nature* **521**, 316-321.
Yaari, G., Bolen, C. R., Thakar, J. and Kleinstein, S. H. (2013). Quantitative set analysis for gene expression: A method to quantify gene set differential expression including gene-gene correlations. *Nucleic Acids Res.* **41**, 1-11.
Yukita, A., Michiue, T., Fukui, A., Sakurai, K., Yamamoto, H., Ihara, M., Kikuchi, A. and Asashima, M. (2004). XSENP1, a novel sumo-specific protease in Xenopus, inhibits normal head formation by down-regulation of Wnt/beta-catenin signalling. *Genes Cells* **9**, 723-736.
Zakin, L., Reversade, B., Virlon, B., Rusniok, C., Glaser, P., Elalouf, J.-M. and Brulet, P. (2000). Gene expression profiles in normal and Otx2−/− early gastrulating mouse embryos. *Proc. Natl. Acad. Sci. USA* **97**, 14388-14393.